2009 IEEE International Conference on Robotics and Automation
Kobe International Conference Center
Kobe, Japan, May 12-17, 2009

Trajectory Generation of Robotic Fingers Based on Tri-axial Tactile Data for Cap Screwing Task

M. Ohka, N. Morisawa, and H. B. Yussof, *Member*, *IEEE*

Abstract— **In a previous paper, we developed a robotic finger equipped with optical three-axis tactile sensors, of which the sensing cell can separately detect normal and shearing forces. With appropriate precision, the robotic finger was able to perform three tasks: scanning flat specimens to obtain the friction coefficient, following the contour of objects, and manipulating a parallelepiped case put on a table by sliding it on the table. In the present study, designed as a follow-up to the above study, a robotic hand is composed of two robotic fingers. Not only tri-axial force distribution directly obtained from the tactile sensor but also the time derivative of the shearing force distribution are used for the hand control algorithm: if grasping force measured from normal force distribution is lower than a threshold, grasping force is increased; the time derivative is defined as slippage; if slippage arises, grasping force is enhanced to prevent fatal slippage between the finger and an object. In the verification test, the robotic hand screws a bottle cap to close it. Although input finger trajectories were a rectangular roughly decided to touch and screw the cap, a segment of the rectangular was changed from a straight line to a curved line to fit the cap contour. We concluded that higher order tactile information such as tri-axial tactile data can reduce the complexity of the control algorithm.**

I. Introduction

Optical three-axis tactile sensors[1]-[4] produced by the authors are superior to other tactile sensors[5]-[10] because they can simultaneously detect normal and shearing forces and because of their sensing ability for detecting contact physics caused between them and an object. Regarding flexible and impact resistant surfaces as the most important, we improved conventional optical waveguide type tactile sensors [11]-[15] to develop the optical three-axis tactile sensor. In a previous paper,[16] we developed a hemispherical tactile sensor for general-purpose use with our three-axis tactile sensor, and the three-axis tactile sensor was mounted on a robotic finger of three degrees of freedom to evaluate the tactile sensor for dexterous hands. Three kinds of experiments were performed. In the first, the robotic finger touches and scans flat specimens to evaluate their friction coefficient. In the second, it detects the contours of parallelepiped and cylindrical objects. Finally, it manipulates a parallelepiped plastic case put on a table by sliding it.

So far several researchers have tried to mount tactile sensors on robotic multi-fingered hands to enhance manipulation and to stabilize grasping objects. Kaneko et al.[14] and Maekawa et al.[15] formulated dynamics including tactile information obtained by a conventional optical waveguide type tactile sensor mounted on the fingertip. These studies are important milestones because they showed the effectiveness of tactile information on multi-fingered hands. However, since tactile sensors used in these studies were of the uni-axis type, Coulomb law is assumed to estimate slippage using a friction cone. Since the friction coefficient is not distributed homogeneously, assumption of a constant friction coefficient causes instability in grasping an object. Additionally, a series of dynamic equations is complicated and requires much numerical calculation time.

On the other hand, our robotic hand can obtain differences in the object's attitude, friction coefficient, and subtle surface unevenness because the three-axis tactile sensor is used instead of the conventional uni-axial tactile sensor. Therefore, the application area will be spread by the equipment of the three-axis tactile sensor. Since our tactile sensor can detect higher order information compared to the uni-axial tactile sensors, the robotic hand's behavior is determined on the basis of tri-axial tactile data with a simplified control algorithm. Not only tri-axial force distribution directly obtained from the tactile sensor but also the time derivative of shearing force distribution is used for the hand control program. If grasping force measured from normal force distribution is lower than a threshold, grasping force is increased. In the program, the time derivative of shearing force is defined as slippage; if slippage arises, grasping force is enhanced to prevent fatal slippage between the finger and an object.

In the present paper, the robotic hand is composed of two robotic fingers, which were developed in the preceding study. Using the robotic hand, we intend to indicate that tri-axial tactile data generate the trajectory of the robotic fingers, even if a simple initial trajectory is provided for the control program. In the verification test, the robotic hand screwed a bottle cap to close it. An experimental apparatus was composed of the two-fingered hand, a bottle holder and a torque sensor to monitor generated torque during the experiment. Variation in torque and generated trajectory were examined to evaluate the present robotic hand and the cap closing algorithm.

M. Ohka is with the Graduate School of Information Science, Nagoya University, Furo-cho, Chikusaku, Nagoya 464-8601, Japan (phone: 81-52-789-4861; fax: 81-52-789-4800; e-mail: ohka@ is.nagoya-u.ac.jp).

N. Morisawa is with Graduate School of Engineering, Nagoya University.

H. B. Yussof is with the Graduate School of Information Science, Nagoya University, Japan (hanafiah@nuem.nagoya-u.ac.jp).

978-1-4244-2789-5/09/$25.00 ©2009 IEEE

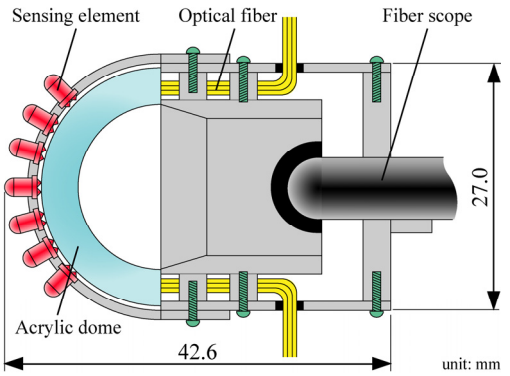

Fig. 1 Fingertip including three-axis tactile sensor

II. Three-axis Tactile Sensor

Since our three-axis tactile sensor has been explained in previous papers,[1]-[3], [16] the structure and functions of the tactile sensor are described briefly in the present paper. The tactile sensor is composed of a CCD camera, an acrylic dome, a light source, and a computer as shown in Fig. 1. The light emitted from the light source is directed into the acrylic dome. Contact phenomena are observed as image data, which are acquired by the CCD camera and transmitted to the computer to calculate the three-axis force distribution. The sensing element presented in this paper is comprised of a columnar feeler and eight conical feelers. The sensing elements, which are made of silicone rubber, are designed to maintain contact with the conical feelers and the acrylic dome and to make the columnar feelers touch an object.

When the three components of the force vector, F_x, F_y, and F_z, are applied to the tip of the columnar feeler, contact between the acrylic dome and the conical feelers is measured as a distribution of gray-scale values, which are transmitted to the computer. F_x, F_y, and F_z values are calculated using integrated gray-scale value G and the horizontal displacement of the centroid of gray-scale distribution. We are currently designing a multi-fingered robotic hand for general-purpose use in robotics. The robotic hand includes links, fingertips equipped with the three-axis tactile sensor, and micro actuators (YR-KA01-A000, Yasukawa). Each micro actuator, which consists of an AC servo-motor, a harmonic drive, and an incremental encoder, is particularly developed for application to a multi-fingered hand. Since the tactile sensors must be fitted to a multi-fingered hand, we are developing a fingertip that includes a hemispherical three-axis tactile sensor.

Sensing elements are arranged on the acrylic dome in a concentric configuration. The acrylic dome is illuminated along its edge by optical fibers connected to a light source. Image data consisting of bright spots caused by the feelers' collapse are retrieved by an optical fiber scope connected to the CCD camera.

Image data acquired by the CCD camera are divided into 41 sub-regions (Fig. 2). The dividing procedure, digital filtering, integrated gray-scale values, and centroid

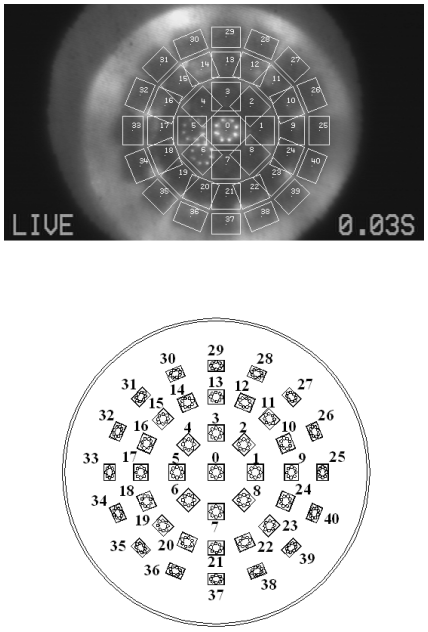

Fig. 2 Image data obtained by CCD camera and address of sensing elements

displacement are processed on an image processing board.

Since the image warps due to projection from a hemispherical surface (Fig. 2), software installed on the computer modifies the warped image data and calculates G, u_x, and u_y to obtain the three-axis force applied to the tip of the sensing element.

III. Kinematics of Robotic Finger

As shown in Fig. 3, each robotic finger has three movable joints. The frame of the workspace is set on the bottom of the z-stage. The kinematics of the present hand is derived according to Denavit-Hartenberg notation shown in Fig. 3. The frame of the workspace is defined as O-*xyz*. The frames of O*i*- $x_i y_i z_i$ ($i = 0,2,\cdots,5$) (in the following, O-*xyz* is used instead of O_0- $x_0 y_0 z_0$) are attached on each joint, the basement of the z-stage, or the fingertip, as shown in Fig. 3. The velocities of the micro actuators ($\dot{\boldsymbol{\theta}} = \begin{pmatrix} \dot{\theta}_1 & \dot{\theta}_2 & \dot{\theta}_3 \end{pmatrix}$) are calculated with

$$\dot{\boldsymbol{\theta}} = \mathbf{J}^{-1}(\boldsymbol{\theta})\dot{\mathbf{r}} \tag{1}$$

to satisfy specified velocity vector $\dot{\mathbf{r}}$ ($= \begin{pmatrix} \dot{x} & \dot{y} & \dot{z} \end{pmatrix}$), which is calculated from the planed trajectory. Jacobian $\mathbf{J}(\boldsymbol{\theta})$ is obtained by the kinematics of the robotic hand as follows:

$$\mathbf{J}(\boldsymbol{\theta}) = \begin{bmatrix} -R_{13}(l_2 + l_3 c_2 + l_4 c_{23}) & l_3(R_{11}s_3 + R_{12}c_3) + l_4 R_{12} & R_{12} l_4 \\ -R_{23}(l_2 + l_3 c_2 + l_4 c_{23}) & l_3(R_{21}s_3 + R_{22}c_3) + l_4 R_{22} & R_{22} l_4 \\ -R_{33}(l_2 + l_3 c_2 + l_4 c_{23}) & l_3(R_{31}s_3 + R_{32}c_3) + l_4 R_{32} & R_{32} l_4 \end{bmatrix}, \tag{2}$$

where

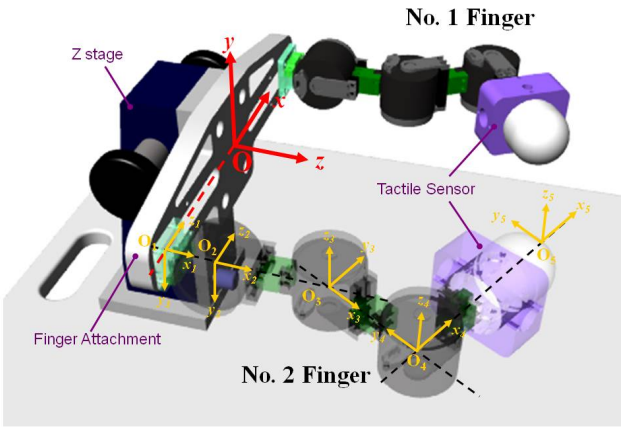

Fig. 3 Robotic hand equipped with three-axis tactile sensors

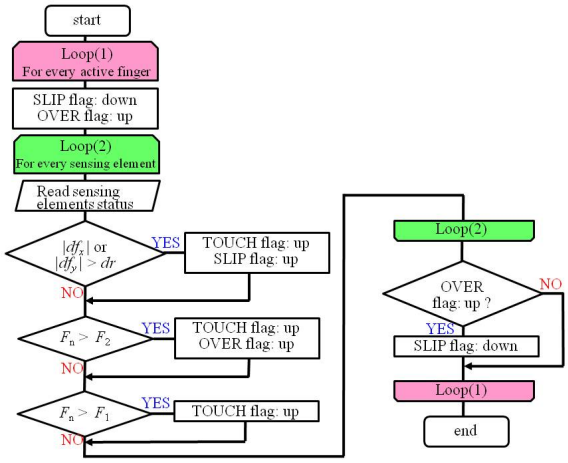

Fig. 4 Algorithm of flag analyzer

$$\begin{bmatrix} R_{11} & R_{12} & R_{13} \\ R_{21} & R_{22} & R_{23} \\ R_{31} & R_{32} & R_{33} \end{bmatrix} = \begin{bmatrix} a_{11}c_{23}+a_{13}s_{23} & -a_{11}s_{23}+a_{13}c_{23} & -a_{12} \\ a_{21}c_{23}+a_{23}s_{23} & -a_{21}s_{23}+a_{23}c_{23} & -a_{22} \\ a_{31}c_{23}+a_{33}s_{23} & -a_{31}s_{23}+a_{33}c_{33} & -a_{32} \end{bmatrix},$$

$$\begin{bmatrix} a_{11} & a_{12} & a_{13} \\ a_{21} & a_{22} & a_{23} \\ a_{31} & a_{32} & a_{33} \end{bmatrix}$$

$$= \begin{bmatrix} c\phi_1 c_1 + s\phi_1 s\phi_2 s_1 & -c\phi_1 s_1 + s\phi_1 s\phi_2 s_1 & s\phi_1 c\phi_2 \\ c\phi_2 s\phi_1 & c\phi_2 s\phi_1 & -s\phi_2 \\ -s\phi_1 c_1 + s\phi_1 s\phi_2 s_1 & s\phi_1 s_1 + c\phi_1 s\phi_2 c\phi_1 & c\phi_1 c\phi_2 \end{bmatrix}$$

$c_i \equiv \cos\theta_i$, $s_i \equiv \sin\theta_i$, $c\phi_i \equiv \cos\phi_i$, $s\phi_i \equiv \sin\phi_i$,

$c_{ij} \equiv \cos(\theta_i + \theta_j)$, $s_{ij} \equiv \sin(\theta_i + \theta_j)$, $(i\,;\ j = 1, 2, 3)$. (3)

In the above equations, the rotations of the first frame around the x_0- and y_0-axes are denoted as ϕ_1 and ϕ_2, respectively. The distance between the origins of the m-th and m+1-th frames is denoted as l_m. The joint angles of the micro actuators on O_2-$x_2y_2z_2$, O_3-$x_3y_3z_3$ and O_4-$x_4y_4z_4$ are θ_1, θ_2, and θ_3, respectively.

Position control of the fingertip is performed based on resolved motion rate control. In this control method, joint angles are assumed at the first step, and displacement vector $\mathbf{r}_0$ is calculated with kinematics. Adjustment of joint angles is obtained by Eq. (4) and the difference between $\mathbf{r}_0$ and objective vector $\mathbf{r}_d$ to modify joint angle $\boldsymbol{\theta}_1$ at the next step. The modified joint angle is designated as the current angle in the next step, and the above procedure is repeated until the displacement vector at k-th step $\mathbf{r}_k$ coincides with objective vector $\mathbf{r}_d$ within a specified error. That is, the following Eqs. (9) and (10) are calculated until $|\mathbf{r}_d - \mathbf{r}_k|$ becomes small enough:

$$\dot{\mathbf{r}}_k = \mathbf{J}\dot{\boldsymbol{\theta}}_k, \quad (9)$$

$$\boldsymbol{\theta}_{k+1} = \boldsymbol{\theta}_k - \mathbf{J}^{-1}(\mathbf{r}_d - \mathbf{r}_k). \quad (10)$$

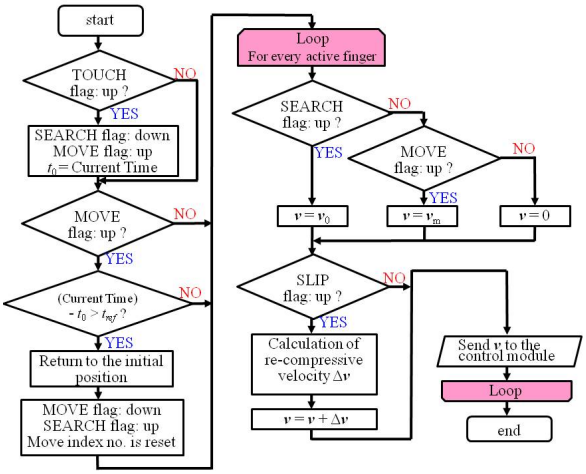

Fig. 5 Algorithm of finger speed estimator

IV. Control Algorithm

Our objective is to show that the robotic hand adapts its finger trajectory to the environment according to tri-axial tactile data. Hence, we make a simple control algorithm for the hand. In the algorithm, there is an assumption that finger trajectory provided beforehand to the hand is as simple as possible. The trajectory is modified to prevent normal force from exceeding a threshold and to stabilize slippage caused on the contact area according to tri-axial tactile data.

The hand is controlled according to velocity control. First, hand status becomes "search mode" to make fingers approach an object with finger speed $\mathbf{v} = \mathbf{v}_0$. After the fingers touch the object, the hand status becomes "move mode" to manipulate the object with finger speed $\mathbf{v} = \mathbf{v}_m$. During both search and move modes, when the absolute time derivative of the shearing force of a sensing element exceeds a threshold dr, this system regards the sensing element as slippage. To prevent the hand from dropping the object, re-compressive velocity is defined as moving the fingertip along the counter direction of applied force.

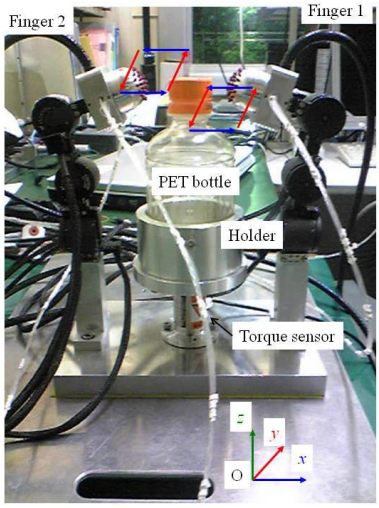

Fig. 7 Roughly designed motion at first

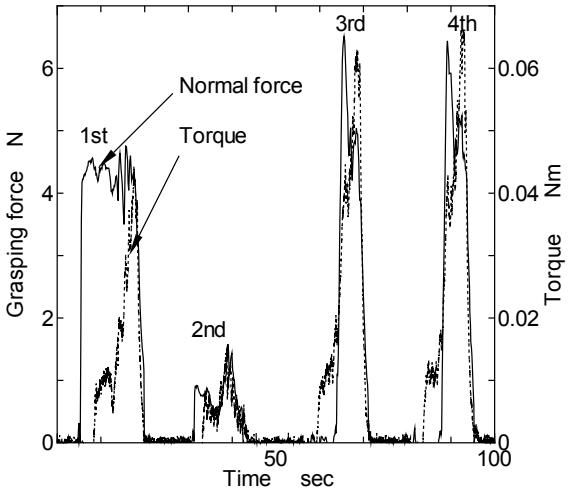

Fig. 8 Relationship between grasping force and torque

However, if normal force of a sensing element exceeds a threshold F_2, the re-compressive velocity is canceled to prevent the sensing element from breaking. The hand is controlled by a control module with applying total velocity obtained by adding the re-compressive velocity to current velocity.

In our system, the sensor control program and hand control program are executed in different computers because CPU time is efficiently consumed using a multi-task program method. These programs are synchronized with the following five flags.

SEARCH: Fingers search for an object with initial finger velocity $\mathbf{v}_0$ until normal force of a sensing element exceeds a threshold F_1 or Slip flag is raised.

MOVE: This flag is raised whenever the robotic hand manipulates an object.

TOUCH: This flag is raised whenever one of the fingers touches an object.

SLIP: This flag is raised whenever the time derivative of shearing force exceeds a threshold dr.

OVER: This flag is raised when normal force of a sensing element exceeds a threshold F_2.

These flags are decided according to tri-axial tactile data and finger motions. Since two modules, the flag analyzer and finger speed estimator, mainly play the role of object handling, these modules are shown in Figs. 4 and 5, respectively.

In the flag analyzer, TOUCH flag, SLIP flag and OVER flag are decided. The flag analyzer regards finger status as touching an object, when normal force of a sensing element exceeds F_1 or the absolute time derivative of the shearing force exceeds dr (SLIP flag is raised). Whenever it regards finger status as touching an object, the TOUCH flag is raised. The OVER flag is raised when normal force of a sensing element exceeds F_2 to prohibit re-compressive motion.

In the finger speed estimator, the velocity of the fingertip is determined based on the five flag values and conserved whenever contact status is not changed. Since the screwing cap problem requires touch and release motion, the MOVE and SEARCH flags are controlled according to the TOUCH flag and time spent. Whenever the SLIP flag is raised, a sensing element of the largest normal force is determined and the re-compressive velocity of the finger is determined as an inward normal line of the sensing element. The re-compressive velocity is added to the current velocity, and the resultant velocity is applied to the control module.

V. Evaluation Experiment

A. Experimental Apparatus

In order to examine the above algorithm, the robotic hand performed the bottle cap closing task because this task requires a curved trajectory along the cap contour. Evaluation of cap closing is performed using an apparatus including a torque sensor. Figure 7 shows the apparatus composed of the two-fingered hand, the torque sensor (TCF-0.2N, Nippon Tokushu Sokki, Co., Ltd.) and a PET bottle holder. A PET bottle is clamped with two screws of the PET holder, and its cap is turned by the robotic hand. The torque sensor measures torque with four strain gauges. Variation in gauge resistance is measured as voltage through a bridge circuit, and it is sent to a computer with an A/D converter to obtain the relationship between finger configuration and generated torque.

B. Experimental Procedure

The experimental apparatus is shown in Fig. 7. A PET bottle is held by the holder as shown in Fig. 7. At first, two fingers approach the cap, and moving direction is changed to the tangential direction of the cap surface after grasping force exceeds 1 N. After the finger moves, keeping the direction within 10 mm, the fingers are detached from the cap surface and returned to each home position from which they start moving. Consequently, the trajectory of the fingers is designed as shown in Fig. 7. During the task of closing the cap, variation in

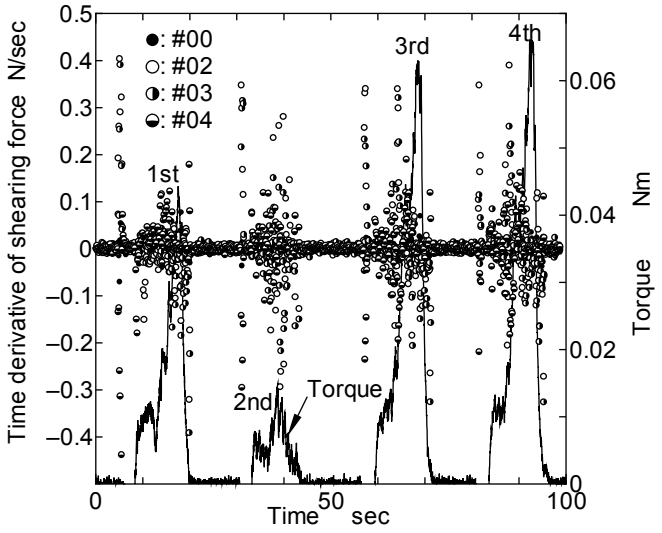

Fig. 9 Relationship between variations in time derivative of shearing force and torque

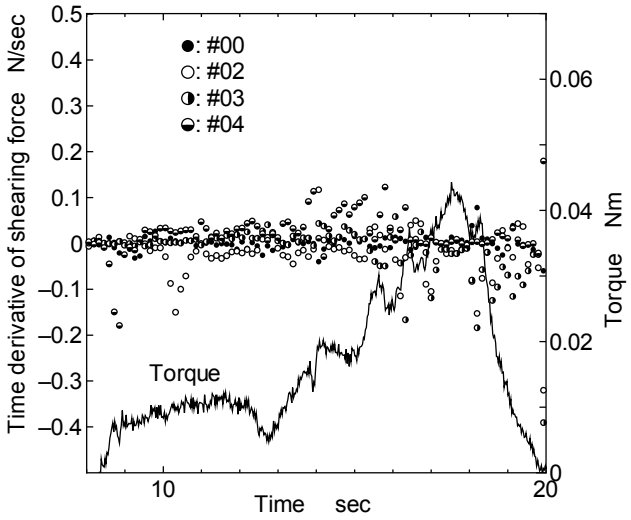

Fig. 10 Detailed relationship between variations in time derivative of shearing force and torque at 1st screwing

torque is monitored through the torque sensor to evaluate the task. Even if the trajectory is simple, we will show that it adapts to the cap contour in the following section.

VI. Experimental Results and Discussion

A. Relationship between grasping force and torque

The relationship between grasping force and torque while screwing the bottle cap is shown in Fig. 8 to overview the experiment. Since touch and release motion is continued four times, four heaps are found in Fig. 8. As shown in Fig. 8, compared to the 1st screwing motion, both grasping force and torque decrease considerably in the 2nd screwing, and in the 3rd and 4th screwings they increase compared to the former two screwings. Since the 3rd and 4th screwings show almost the same variations in grasping force and torque, screwing seems to become constant. Therefore, after the 3rd screwing, the cap seems to be closed. In the 1st screwing, we can observe the transition from light screwing to forced screwing because torque increases in spite of constant grasping force. It is shown that the cap is turned without resistant torque at first. The reason for reducing grasping force and torque in the 2nd screwing is the variation in contact position and status between the 1st and 2nd screwings. Screwing the cap is successfully completed as mentioned above.

B. Relationship between time derivative of shearing force and torque

When the cap is screwed completely, slippage between the robotic finger and the cap occurs. To examine this phenomenon, the relationship between the time derivative of the shearing force and torque is shown in Fig. 9. As shown in Fig. 9, the time derivative of the shearing force shows periodic bumpy variation. This bumpy variation synchronizes with variation in torque. This means large tangential force induces the time derivative of the shearing force, which is caused by the trembling of the slipping sensor element.

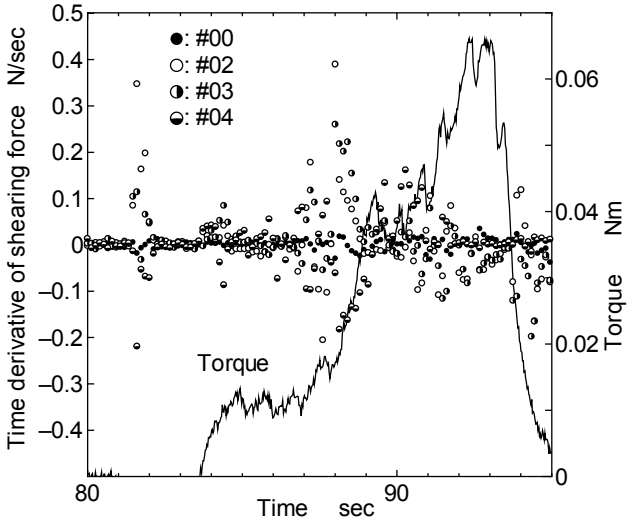

Fig. 11 Detailed relationship between variations in time derivative of shearing force and torque at 4th screwing

To examine screwing the cap, a comparison between the results of the 1st screwing and 4th screwing is performed with Figs. 10 and 11. In the 1st screwing, since the cap is loose, the marked time derivative of the shearing force does not occur in Fig. 10. On the other hand, in the 4th screwing, the marked time derivative of the shearing force does occur because of the locking of the cap.

From the above discussion, the robotic hand can screw the bottle cap to close the cap. Additionally, the time derivative of the shearing force can be adopted as a measure for screwing the cap.

C. Trajectory of fingertip modified according to tri-axial tactile data

Trajectories of sensor element tips are shown in Figs. 12 and 13. If the result of Fig. 12 is compared with the result of Fig. 13, trajectories of Fig. 13 are more close to the cap

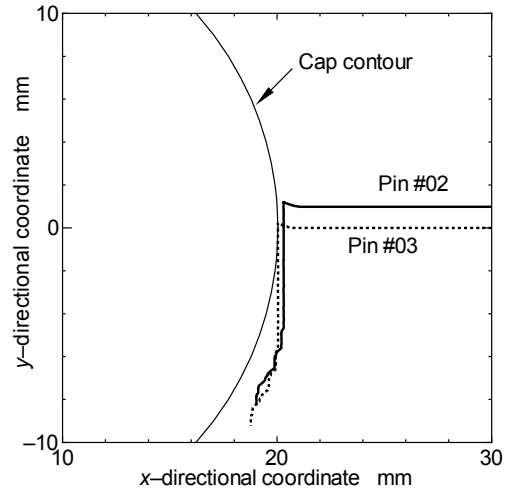

Fig. 12 Trajectories of sensor element before closing the cap

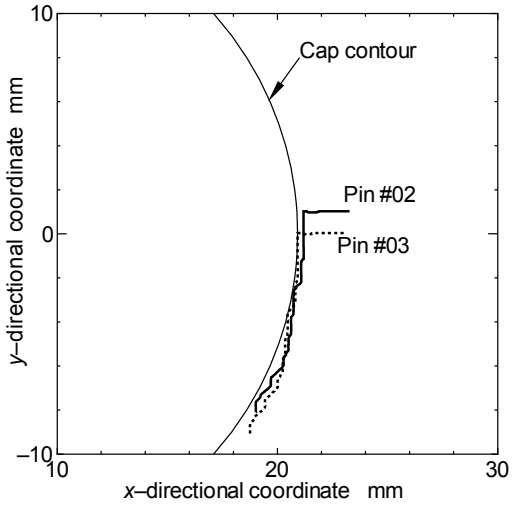

Fig. 13 Trajectories of sensor element after closing the cap

contour. Modification of the trajectory is saturated after closing the cap. Although input finger trajectories were a rectangular roughly decided to touch and turn the cap as described in the previous section, a segment of the rectangular was changed from a straight line to a curved line to fit the cap contour.

VII. Conclusion

In the present paper, a robotic hand is composed of two robotic fingers to indicate that tri-axial tactile data generate the trajectory of the robotic fingers. Since our tactile sensor can detect higher order information compared to the other tactile sensors, the robotic hand's behavior is determined on the basis of tri-axial tactile data. Not only tri-axial force distribution directly obtained from the tactile sensor but also the time derivative of shearing force distribution is used for the hand control program. If grasping force measured from normal force distribution is lower than a threshold, grasping force is increased. The time derivative is defined as slippage; if slippage arises, grasping force is enhanced to prevent fatal slippage between the finger and an object. In the verification test, the robotic hand rotates a bottle cap to close it. Although input finger trajectories were a rectangular roughly decided to touch and turn the cap, a segment of the rectangular was changed from a straight line to a curved line to fit the cap contour. Therefore, higher order tactile information can reduce the complexity of the control program.

Acknowledgment

This study was partly supported by 2008 JSPS (Japan Society for the Promotion of Science) Postdoctoral Fellowship for Foreign Researchers (No. 20-08062).

References

[1] Ohka, M., Mitsuya, Y., Matsunaga, Y., and Takeuchi, S., "Sensing Characteristics of an Optical Three-axis Tactile Sensor Under Combined Loading," Robotica, vol. 22, 2004, pp. 213-221.

[2] Ohka, M., Kawamura, T., Itahashi, T., Miyaoka, T., and Mitsuya, Y., "A Tactile Recognition System Mimicking Human Mechanism for Recognizing Surface Roughness," JSME International Journal, Series C. Vol. 48, No. 2, 2005, pp. 278-285.

[3] M. Ohka, Y. Mitsuya, I. Higashioka, H. Kabeshita, "An Experimental Optical Three-axis Tactile Sensor for Micro-Robots," Robotica, vol. 23-4, 2005, pp. 457-465.

[4] Raibert, H. M. and Tanner, J. E., "Design and Implementation of a VSLI Tactile Sensing Computer," Int. J. Robotics Res., Vol. 1-3, 1982, 3-18.

[5] Hackwood, S., Beni, G., Hornak, L. A., Wolfe, R. and Nelson, T. J., "Torque-Sensitive Tactile Array for Robotics," Int. J. Robotics Research, Vol. 2-2, 1983, pp. 46-50.

[6] Dario, P., Rossi, D.D., Domenci, C. and Francesconi, R., "Ferroelectric Polymer Tactile Sensors with Anthropomorphic Features," Proc. 1984 IEEE Int. Conf. On Robotics and Automation, 1984, pp. 332-340.

[7] Novak, J. L., "Initial Design and Analysis of a Capacitive Sensor for Shear and Normal Force Measurement," Proc. of 1989 IEEE Int. Conf. on Robotic and Automation, 1989, pp. 137-145.

[8] Nicholls, H. R. & Lee, M. H., "A Survey of Robot Tactile Sensing Technology," Int. J. Robotics Res., Vol. 8-3, 1989, pp. 3-30.

[9] Ohka, M. et al., "Tactile Expert System Using a Parallel-fingered Hand Fitted with Three-axis Tactile Sensors," JSME Int. J., Series C, Vol. 37, No. 1, 1994, pp. 138-146.

[10] Takeuchi, S., Ohka, M., and Mitsuya, Y., "Tactile Recognition Using Fuzzy Production Rules and Fuzzy Relations for Processing Image Data from Three-dimensional Tactile Sensors Mounted on a Robot Hand," Proc. of the Asian Control Conf., Vol. 3, 1994, pp. 631-634.

[11] Mott, H., Lee, M. H. and Nicholls, H. R., "An Experimental Very-High-Resolution Tactile Sensor Array," in Proc. 4th Int. Conf. On Robot Vision and Sensory Control, 1984, pp. 241-250.

[12] Tanie, K., Komoriya, K., Kaneko M., Tachi, S., and Fujiwara, A., "A High-Resolution Tactile Sensor Array," Robot Sensors Vol. 2: Tactile and Non-Vision, Kempston, UK: IFS (Pubs), 1986, pp. 189-198.

[13] Nicholls, H. R., "Tactile Sensing Using an Optical Transduction Method," Traditional and Non-traditional Robot Sensors (Edited by T. Fig. C. Henderson), Springer-Verlag, 1990, pp. 83-99.

[14] Kaneko, M., H. Maekawa, and K. Tanie, Active Tactile Sensing by Robotic Fingers Based on Minimum-External-Sensor-Realization, Proc. of IEEE Int. Conf. on Robotics and Automation, pp. 1289-1294, 1992.

[15] Maekawa, H., Tanie, K., Komoriya, K., Kaneko M., Horiguchi, C., and Sugawara, T., "Development of a Finger-shaped Tactile Sensor and Its Evaluation by Active Touch," Proc. of the 1992 IEEE Int. Conf. on Robotics and Automation, 1992, pp. 1327-1334.

[16] M. Ohka, N. Morisawa, H. Suzuki, J. Takada, H. Kobayashi, H. Yussof, "A Robotic Finger Equipped with an Optical Three-axis Tactile Sensor," Proc. of IEEE Inter. Conf. on Robotic and Automation, 2008, pp. 3425-3430.